Hindawi
Complexity
Volume 2019, Article ID 6450853, 11 pages
https://doi.org/10.1155/2019/6450853

Research Article

Dynamic Characteristics of Metro Tunnel Closely Parallel to a Ground Fissure

Nina Liu,[1,2,3] **Quanzhong Lu**,[1,2] **Xiaoyang Feng**,[1] **Wen Fan**,[1,2] **Jianbing Peng**,[1,2] **Weiliang Liu**,[1,4] **and Xin Kang**[1,5]

[1]*Key Laboratory of Western China's Mineral Resource and Geological Engineering, Ministry of Education, Chang'an University, Xi'an 710054, China*
[2]*Key Laboratory of Mine Geological Hazards Mechanism and Control, Chang'an University, Xi'an 710054, China*
[3]*School of Geological Engineering and Geomatics, Chang'an University, Xi'an 710054, China*
[4]*School of Marine Sciences, Sun Yat-Sen University, Guangzhou 510275, China*
[5]*College of Civil Engineering, Hunan University, Changsha, 410082, China*

Correspondence should be addressed to Nina Liu; dcdgx16@chd.edu.cn and Quanzhong Lu; dcdgx14@chd.edu.cn

Received 8 February 2019; Accepted 1 April 2019; Published 10 April 2019

Academic Editor: Guang Li

Shaking table model test and numerical simulation model were conducted on scaled tunnel model to investigate the mechanism and effect of seismic loadings on metro tunnel which is closely parallel to an active ground fissure. Key technical details of the experimental test were set up; for example, similarity relations, boundary conditions, sensors layout, and modelling methods were presented. Synthetic wave, El Centro wave, and Kobe wave were adopted as the input earthquake waves. Results measured from shaking table model and numerical model were compared and analyzed. It is found that the fissure increased the dynamic response features as accelerations and strains of the tunnel, especially in the part close to the fissure. Average incremental percentage of acceleration amplifying coefficient was 8.33% from the wall close to fissure than the symmetrical one. The short distance to fissure led to serious circumferential dynamic strain, while the distance to fissure influenced the axial dynamic strain less. The numerical analysis results have a good correspondence with those of the shaking table model test. The waves at the top of tunnel have more scattering and emission effect. The fissure increases the dynamic response of the tunnel close to it.

1. Introduction

The geological characteristic is an important aspect in underground engineering. The geohazards as faults, ground fissures, and landslides are all influencing the engineering design, construction, and building in lifetime for their special geological structure characteristics. The ground fissure is a kind of geological disaster with activities usually controlled by tectonic movements and extraction of groundwater. The activities of ground fissures influence the underground structures located nearby. The earthquake usually increases the activities of fissures and leads to damage of structures. But the influence of the underground structures in the fissure site by earthquakes is rarely known.

Xi'an city locates in the Fenwei basin with 14 fissures spread in the whole city. From field survey in the past twenty years, the original reason and distribution characteristics had been found. The directions of the fissures are all controlled by Lingtong-Chang'an fault locating at the south margin of Xi'an city. The directions of the fissures are all North-East-East (NEE). The distance between each other is from 500 m to 1500 m. The length of fissures is up to 150 km. with 250 km^2 covering area all over the city. The ground fissure has the three-dimensional dynamical characteristic, as the vertical settlement, the horizontal extension, and the twisting. The ratio of the three movements is 1:0.30:0.03. The vertical settlement is the most serious one.

For the safety, the distance between buildings and fissures had been limited by the design code of the ground fissure site. But it is hard to keep the safety distance in the metro tunnel design. For the Xi'an city a metro system with 23 lines has been planned. The metro system covers the whole city with

Table 1: Parameters of strata and fissure.

Strata	Density γ/(kN·m^{-3})	Young's modulus E/ (MPa)	Poisson ratio μ	Cohesion c/(kPa)	Internal friction angle φ/(°)
Loess	17.5	12.2	0.35	30.0	21.5
Paleosol	19.5	13.5	0.30	35.0	22.0
Silty clay	19.8	20.0	0.32	40.0	25.0
Fissure soil	16.0	2.44	0.35	12.0	18.0

total length up to 986 kilometers. The metro tunnels have different location relationship with fissures, such as being parallel in short distance, intersecting in different angles and, so on [1–5]. It is important to design the metro system to resistant the influence from activities of fissures.

According to the history records, Xi'an city has lots of earthquakes with high intensity. The total number of earthquakes above 4 Ms is 128 times, with 25 times above 5 Ms. since 2 B.C. form the reports of Earthquake Agency, the number of earthquakes is 172 times in 2012, 182 times in 2013, 357 times in 2014, 281 times in 2015, 313 times in 2016, and 263 times in 2017. The earthquakes in recent years influenced the life of citizens. For example, parts of the Xi'an citizens had obviously shake feeling in the earthquake procedure that had 3.0 Ms. intensity on 13 June 2018.

The earthquake design is essential in the underground structures. But they were paid less attention during the past decades till serious disastrous earthquake happened at the Dakai subway station, Japan, 1995. There were more than 30 piles damaged in Kobe earthquake [6, 7]. More researches have been applied for the underground structures safety design in earthquake resistance since then. It was found that the dynamic response characteristics were quite different between the ground and underground structures of earthquake [8–11]. Jesmani et al. and Angin indicated that earthquakes can damage tunnels especially in geohazard sites such as faults, changing strata, and ground fissures [12, 13]. The San-I No. 1 tunnel located 8 km away from the Chelungpu Fault was severely damaged in the Chi-Chi earthquake in 1999. The Longxi tunnel and Zipingpu tunnel of the Duwen highway were crossing two faults as F8 and F11. Both of them had serious damage as lining cracking, joint staggering, and inverted arch uplifting on 12 May 2008 Wenchuan earthquake. The Chengdu subway had obvious damage in the shield tunnel as lining cracks, dislocations, and leakages in Wenchuan earthquake, too[14].

Xi'an is in the 8 Ms. zone in the seismic ground motion parameters zonation map of China, so seismic design must be considered in the city. At the same time, 14 ground fissures are still active with the annual increase rate of about 2~16 mm/a. Previous investigations have shown that a series of damage in the ground and underground structures had been caused by the ground fissures [1–3].

For the geohazard sites as ground fissures and faults, research has been applied to discover the influence from them. The results indict that underground structures as the metro tunnel is influenced not only by the seismic activities but also by the activities of the geological site. Peng et al. simulated the influence of ground fissure activities of strata subsidence by numerical method analysis [2]. The integrity of the site had been impacted and the secondary fissure appeared during the settlement in the fissure site. Liu et al. studied the acceleration response, the soil pressure, and strain responses of shield tunnel and tunnel with segment joints from earthquake in fissure site by shaking table test and numerical simulation analysis [1, 3]. The model tests on the tunnel were focused on the dynamic response characteristics in different soil strata and fissure. With the tunnel crossing the ground fissure, the acceleration, stress, and strain were all increased in the parts close to the fissure. With the flexible joints, the acceleration, stress, and strain optimize a lot. The stress, strain, and acceleration did not increase as much as those in the integrated tunnel. The flexible joints improved the dynamic response of the tunnel in the fissure site. Cheng et al. researched segment tunnel in cycling load in detail. The safety length and damping layer of the tunnel based on the results of model test and numerical simulation analysis have been got [15]. However, the dynamic response characteristics as the acceleration, strain, and stress of tunnel in different location relationship and distance to fissures are essential. But less research of the tunnel parallel to fissures has been applied.

This study investigated the dynamic response as the acceleration, strain, and stress of a metro tunnel parallel to an active ground fissure in short distance when subjected to earthquake by shaking table model and numerical simulation model. El Centro earthquake wave, Kobe earthquake wave, and synthetic Xi'an earthquake wave were applied in tests. The acceleration and the tunnel strain were examined. The results will provide a scientific basis for subway engineering in ground fissure site.

2. Experimental Setup and Procedure

2.1. Engineering Background. Xi'an metro 3rd line is designed in a close proximity of the f_7 ground fissure at Jixiangcun-Xiaozhai site (Figure 1). Figure 2 depicts the strata and the fissure profile of the research site by the drilling points as ZK1-1, ZK1-2, and ZK1-3. The strata are plain fill loess Q_4^{ml}, upper pleistocene aeolian loess Q_3^{eol}, residual paleosolic Q_3^{el}, and middle pleistocene alluvial silty clay Q_2^{al} from top to bottom. The metro tunnel locates at the strata of Q_2^{al} silty clay. The parameters of the strata and fissure are show in Table 1. The tilt of the fissure is 80° and the fissure is filled with silty and fine sand. The f_7 fissure had serious activities as 35.0 mm/a at the construction site from the field survey. And it is forecasted that the total subsidence is up to 300 mm in the coming 100 years [2, 4, 5].

Table 2: Similar constants of shaking table model.

Physical quantity	Similarity relationship	Similar ratio
Length l	C_l	1/30
Displacement u	$C_u = C_l$	1/30
Density ρ	C_ρ	1
Young's modulus E	C_E	1/10
Strain ε	$C_\varepsilon = 1$	1
Stress σ	$C_\sigma = C_E$	1/10
Poisson ratio μ	$C_\mu = 1$	1
Acceleration a	$C_a = C_E(C_l C_\rho)^{-1}$	3
Frequency f	$C_f = \left(C_E/C_\rho\right)^{1/2} C_l^{-1}$	$3\sqrt{10}$
Time t	$C_t = C_l\left(C_\rho/C_E\right)^{1/2}$	$1/3\sqrt{10}$

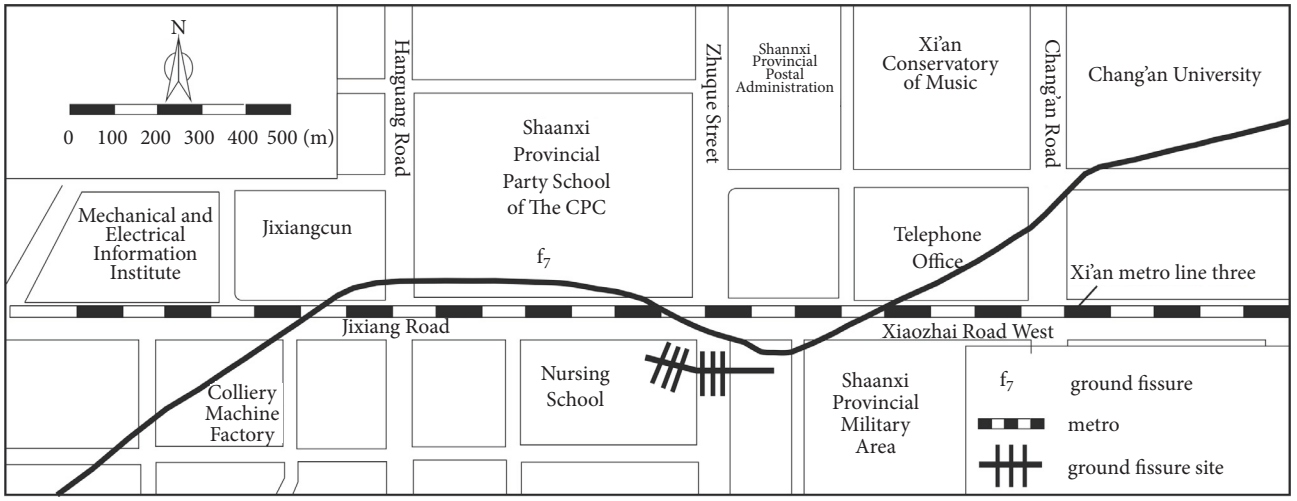

Figure 1: Map of Xi'an metro 3rd line and fissure f_7 on Jixiangcun-Xiaozhai site.

2.2. Shaking Table Model Design. A shear laminar box with length of 3000 mm (shaking direction), 1500 mm width, and 1200 mm height was designed to perform the tests. Three kinds of boundary have been designed in the model box in order to reduce undesirable reflections of dynamic waves from the container boundaries. The sliding boundary was made of polystyrene foam with thickness as 50 mm. It was parallel to the shaking direction, and it was placed on the interior wall of the container to absorb elastic waves reflecting at boundaries. The flexible boundary was made of rubber membrane with the thickness of 2 mm. It was put inside the box wall which was perpendicular to the shaking direction. The friction boundary was made of 10 wood pieces which were nailed at the bottom of model box with distances of 250 mm apart [16–18]. To prepare the model soil layer, a tamping method was used. The soil was poured in layers 150 mm and hammered to 100 mm and each layer was artificially compacted by a hammer. The surface of each layer was brushed to increase the friction and make sure the soil was simulated following the construction site.

Based on the testing capability of the shaking table, the container size, and the strata of prototype site, the geometry similitude ratio was set to be 1/30. The size, density, and elastic modulus are the key principles of the simulation design. The geometric similarity constant was $C_l = 30$, density similarity constant $C_\rho = 30$, and modulus of elasticity $C_E = 30$. Other physical features were determined by the Bockingham's π theorem and dimensional analysis [19]. The dynamic effect is greater than the gravity effect from the experimental studies. With less ballast of the shaking table test, the model can obtain precise measurement data and realistic results. The gravity distortion was considered in the model design with the geometric similarity and kinematic and dynamic similarity [20]. The similarity relationship and similar ratio of the model are listed in Table 2.

The soil of the model was got from the construction site. The water content and the density of the soil were following the prototype site. The fissure was simulated by fine sand according with the field survey. The width of the fissure was 25 mm, with the tilt angle 80°. Figure 3 depicts the model.

The model tunnel was simulated following similarity relationship in Table 2. Based on the material test, the ratio was the following: Plaster:Water:Barite Powder=1:1:3.95. The rebar was simulated by the aluminum wire mesh according to the equal strength principle [15, 21] . Figure 4 is the production procedure of the model tunnel. The model is

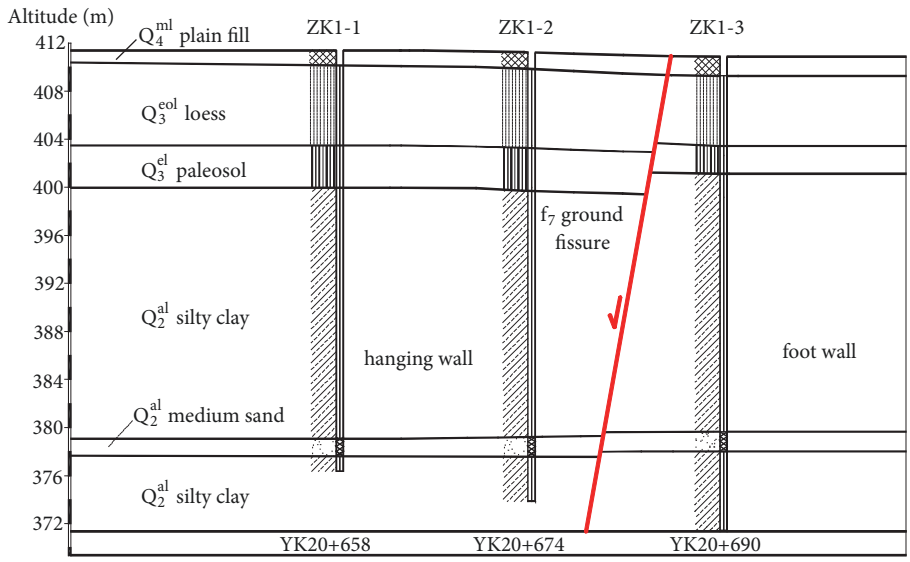

Figure 2: Typical strata of ground fissure f_7.

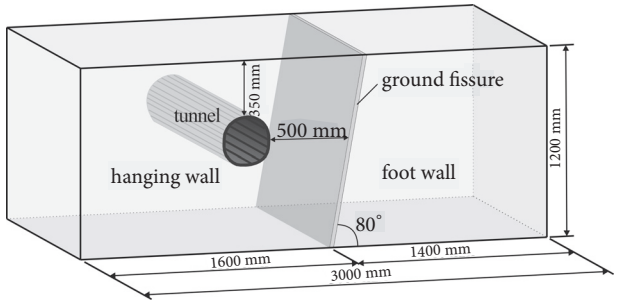

Figure 3: Model test box.

combined of inner and outer parts. Figure 4(a) is the inner template. Figure 4(b) is the aluminum wire mesh which was fixed by the inner template; the distance between them would format the protective layer for model tunnel. Figure 4(c) is the outer template of the tunnel. The thickness of the tunnel which was filled with the combination material was limited by the outer and inner templates. Then the model was cured following the concert cure. After one month, the inner and outer templates were moved; then the model tunnel is shown in Figure 4(d).

2.3. Monitor Points and Dynamic Loading. Figure 5 depicts the location of the acceleration transducers and strain gauges in the model tunnel. The YD-31D acceleration transducer was used to record acceleration data in earthquakes. Four acceleration transducers were fixed out of the tunnel at the points as the bottom, the top, the middle of both walls and named as A1, A2, A3, and A4 in Figure 5(a). The strain gauge was BX120-5AA (50 mm×3 mm) sticking on the outer of the model tunnel. The gages were positioned along the circumference of the tunnel, and at 45° angle distance with each other. The locations of the gages are shown in Figure 5(b).

The input seismic waves were the synthetic Xi'an wave, El Centro earthquake wave, and Kobe earthquake wave. The synthetic Xi'an wave was artificial stimulation of the earthquake in Xi'an city. The El Centro wave was recorded in Empire Valley, USA in 1940. Kobe earthquake wave was recorded in Japan 1995. These waves match with the geological structure of Xi'an city. Figure 6 shows the acceleration time histories and Fourier spectra of the three waves. The earthquake waves were adjusted to accord with the peak acceleration as 0.1 g, 0.15 g, 0.3 g, 0.45 g, and 0.6 g. The white noise with peak acceleration of 0.03 g was loaded to check the natural vibration frequency of the model box before each changing stage of the earthquake waves.

2.4. Numerical Simulation Analysis Model. Figure 7 is the numerical simulation analysis model in FLAC 3D. The size of the numerical model was 3 m (length) × 1.2 m (height). The plain strain was applied in the numerical analysis. The boundary at the bottom was viscous boundary, and other boundaries were free-field boundaries which were simulating the infinite field. The constitutive model of the numerical analysis was ideal elastoplastic constitutive model. Mohr-Coulomb yielding criterion was applied for the yielding criterion. The fissure was following the silty sand characteristic as the test. The tunnel was simulated by entity unit as elastic constitutive. The parameters of the numerical model site and tunnel are shown in Table 3. The contact elements are utilized among the tunnel, fissure, and soil boundaries. The synthesis Xi'an earthquake wave was applied in the numerical model with the peak acceleration as 0.15 g. The duration of the wave was 3.5 s, and the compression ratio of the time was 9.52.

3. Analysis of Test Results

3.1. Response of Acceleration. The acceleration amplifying coefficient is the recorded peak acceleration dividing the corresponding input peak acceleration. Figure 8 shows the

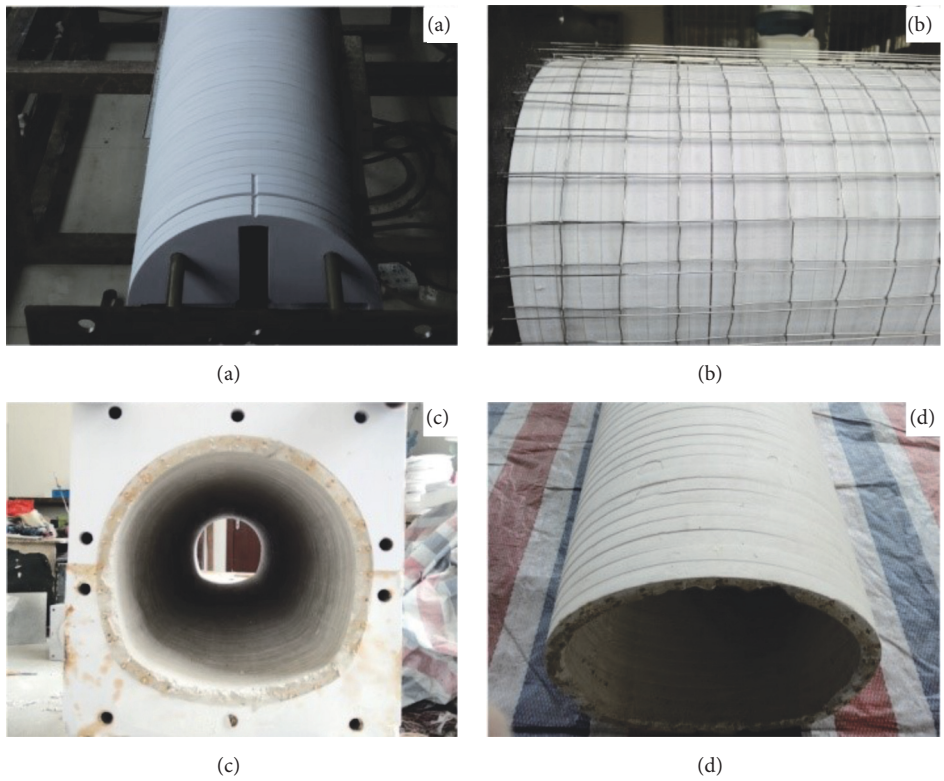

Figure 4: The manufacturing procedure of model tunnel.

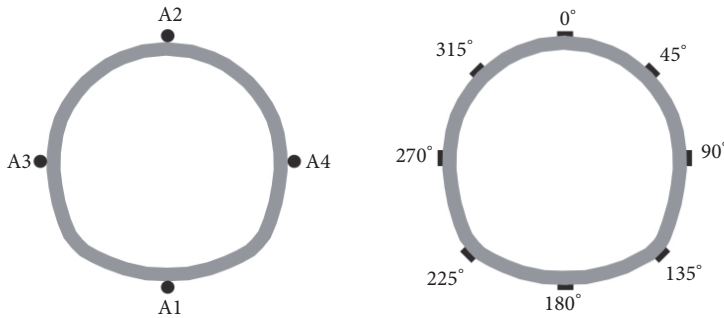

(a) Acceleration transducer position (b) Strain gage position

Figure 5: Monitor points of tunnel (unit: mm).

acceleration amplifying coefficient in the tunnel from shaking table test when the input peak earthquake acceleration was 0.1g, 0.15 g, and 0.3 g of synthesis Xi'an, El Centro, and Kobe earthquake waves. The acceleration amplifying coefficients were different at four monitor points. When the peak acceleration of the input earthquake wave was 0.1 g, the acceleration amplifying coefficients were the biggest at the four points in the El Centro earthquake wave; those of the Kobe wave were the least one. The acceleration amplifying coefficient at the bottom of the tunnel was bigger than that on the top of the model tunnel in the same earthquake (Figure 8(a)). The biggest coefficient was 1.34 got from the bottom of the tunnel in El Centro earthquake. The acceleration amplifying coefficient on the right wall (90°) was a little bigger than that of the symmetrical left wall (270°). With the increase of the peak acceleration, Figure 8(b) depicts the acceleration amplifying coefficient of the tunnel when the peak acceleration was 0.15 g; the acceleration amplifying coefficient in the synthesis Xi'an wave was the biggest. The acceleration amplifying coefficients on the right wall (90°) were bigger than those on the left wall (270°) in the three earthquakes. For example, the acceleration amplifying coefficient was 1.05 on the right wall (90°) when it was 1.02 on the left wall (270°) in the synthesis Xi'an wave. And it was 0.835 and 0.963 on the right wall (90°) when it was 0.816 and 0.625 on the left wall (270°) in the El Centro and Kobe, respectively. The right wall had the biggest acceleration amplification factor in all of the earthquake waves. Figure 8(c) shows the acceleration

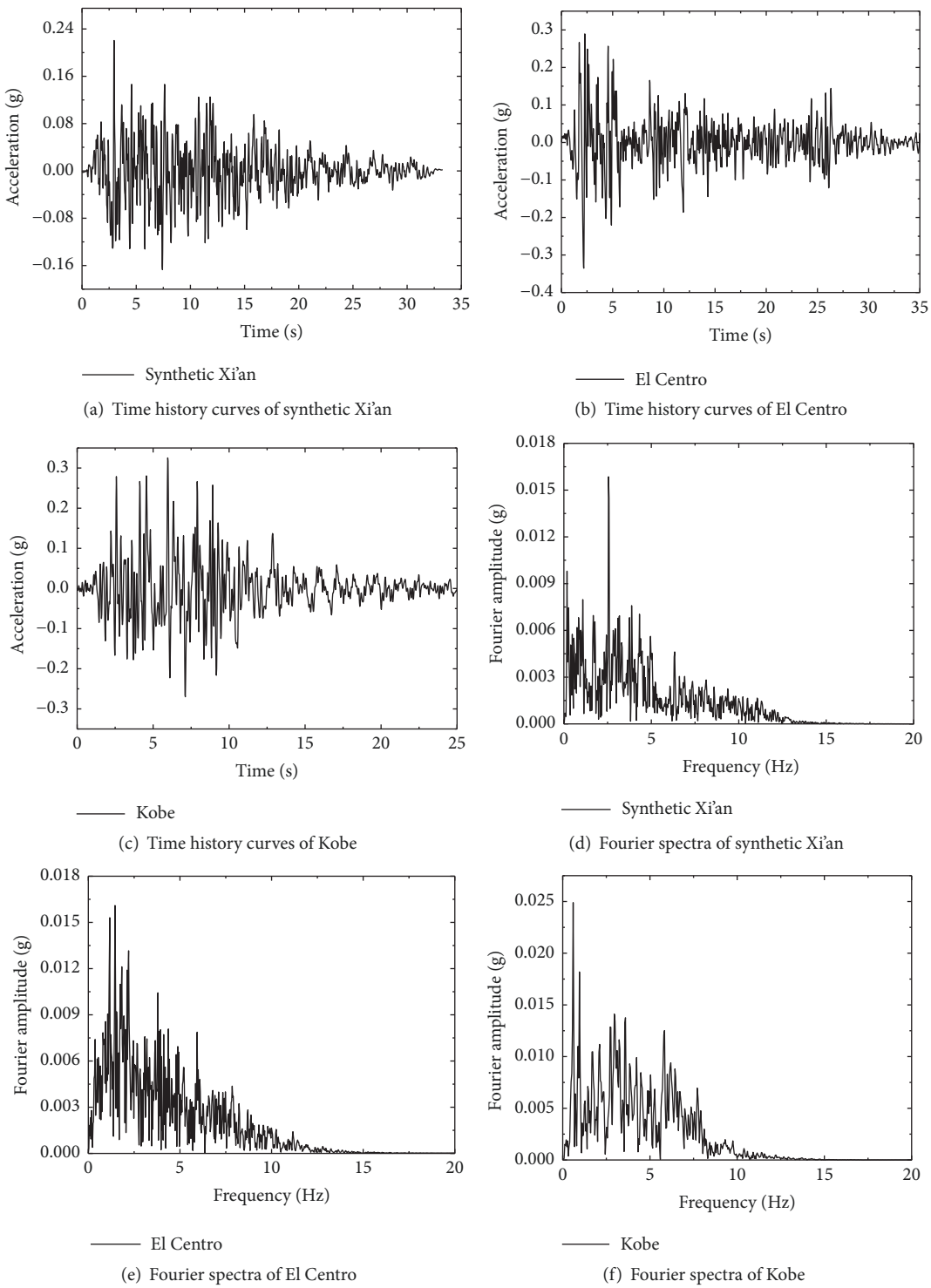

Figure 6: Time-histories and Fourier spectra of input earthquake waves.

amplifying coefficient when the peak acceleration was 0.3 g. The acceleration amplifying coefficient at the right wall (90°) was a little bigger than that of the left wall (270°) in the three earthquakes. It was 1.037, 0.812, and 1.12 on the right wall (90°) when it was 0.946, 0.735, and 1.09 on the left wall (270°) in the three earthquakes, respectively. And the acceleration amplifying coefficient at the bottom of the tunnel (180°) was bigger than that at the top of the tunnel (0°).

Figure 8 indicates that the rule of acceleration amplifying coefficient is similar in the four points. The bottom of the tunnel had the bigger acceleration amplifying coefficient than that at the top of tunnel. The right wall had the bigger

Table 3: Parameters of numerical model.

Geomaterial	Density γ/(kN·m^{-3})	Young's modulus E/ (MPa)	Poisson ratio μ	Cohesion c/(kPa)	Internal friction angle φ/(°)
Site soil	17.9	12.2	0.35	28	21.5
Fissure sand	19.0	10.0	0.28	0	30
Model tunnel	23.5	3000.0	0.2	/	/

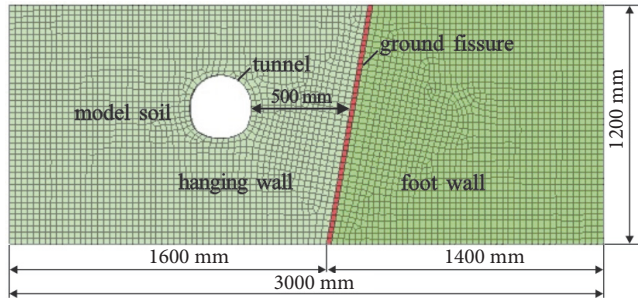

Figure 7: Schematic diagram of numerical simulation.

acceleration amplifying coefficient than that of the left wall. The right wall was more close to the fissure, so the fissure influenced the transport of the earthquake wave and led to the bigger acceleration amplifying coefficient. The more close to the fissure the more the acceleration amplifying coefficient. Average incremental percentage of acceleration amplifying coefficient was 8.33% from right wall to left wall. In the design of the tunnel in fissure site, the bottom and the wall close to the fissure should be paid more attention.

3.2. Tunnel Deformation. The deformation was monitored by strain as mentioned in Figure 5(b). The dynamic strain is the deformation increment that is the biggest deformation subtracting the initial deformation value wave at one monitor point of the tunnel in the correspondence earthquake. Figure 9 depicts the dynamic strain in earthquake waves with the peak acceleration being 0.3 g. Figure 9(a) shows the circumferential dynamic strain and Figure 9(b) is the axial dynamic strain. The dynamic strain of the tunnel in the Kobe wave was the biggest, that of the synthesis Xi'an wave was the least, and the El Centro wave led to the medium circumferential and axial strain of tunnel.

Figure 9(a) shows the circumferential dynamic strain in the tunnel. The strains in the right part of the tunnel were bigger than those at the left symmetrical points. For example, the circumferential dynamic strain at the point of 45° was bigger than that at the 315° point, the same at the 90° compared to that at 270° and the 135° to that of 225°. The biggest circumferential dynamic strain was 108 at the right wall (90°), while the least one was 18 at the 315° points of the tunnel. So the conclusion may get that the right part of the tunnel which was close to the fissure had serious circumferential dynamic strain than that of the left part which was far away from the fissure.

The axial dynamic strain in Figure 9(b) shows that they were bigger on the left and right walls than those of the other six points. And the axial dynamic strains at the right and left wall were approximately equal. The axial dynamic strain did not have the same rule as that of the circumferential dynamic strain, for the influence of distance to the axial strain was less than that to the circumferential.

3.3. Numerical Simulation Analysis Result. Figure 10 shows the input wave and monitor record wave at the bottom of the numerical analysis model. By comparing, the input and record waves had the same peak acceleration values. The record wave followed the input one in the wave shape and the time history process.

Figure 11 shows the acceleration time history curves of the four monitor points of the tunnel in the synthesis Xi'an earthquake wave. The record acceleration time history curves had a good correspondence with the input earthquake wave as the principle from Figure 10. The acceleration changed by time at each point. The curves were similar with what were recorded at the bottom (A1), right wall (A3), and left wall (A4) of the tunnel. But the curves recorded from the top of the tunnel (A2) were different with others. The waves at the top of tunnel had more scattering and emission effect. The waves superposed with each other at the top of the tunnel in traveling process from bottom to top in the fissure site. The superposition effect influenced the wave shape at the top of the tunnel.

3.4. Result Comparison of Numerical and Shaking Table Model. Figure 12 depicts the peak accelerations at different tunnel points from numerical simulation analysis model and shaking table test. The peak acceleration values were similar with each other based on the two methods. The principles of peak acceleration were similar in both models. The peak acceleration on the right wall of the tunnel was the biggest, while the right part was close to the ground fissure. The peak acceleration on the left wall was less than that of the right

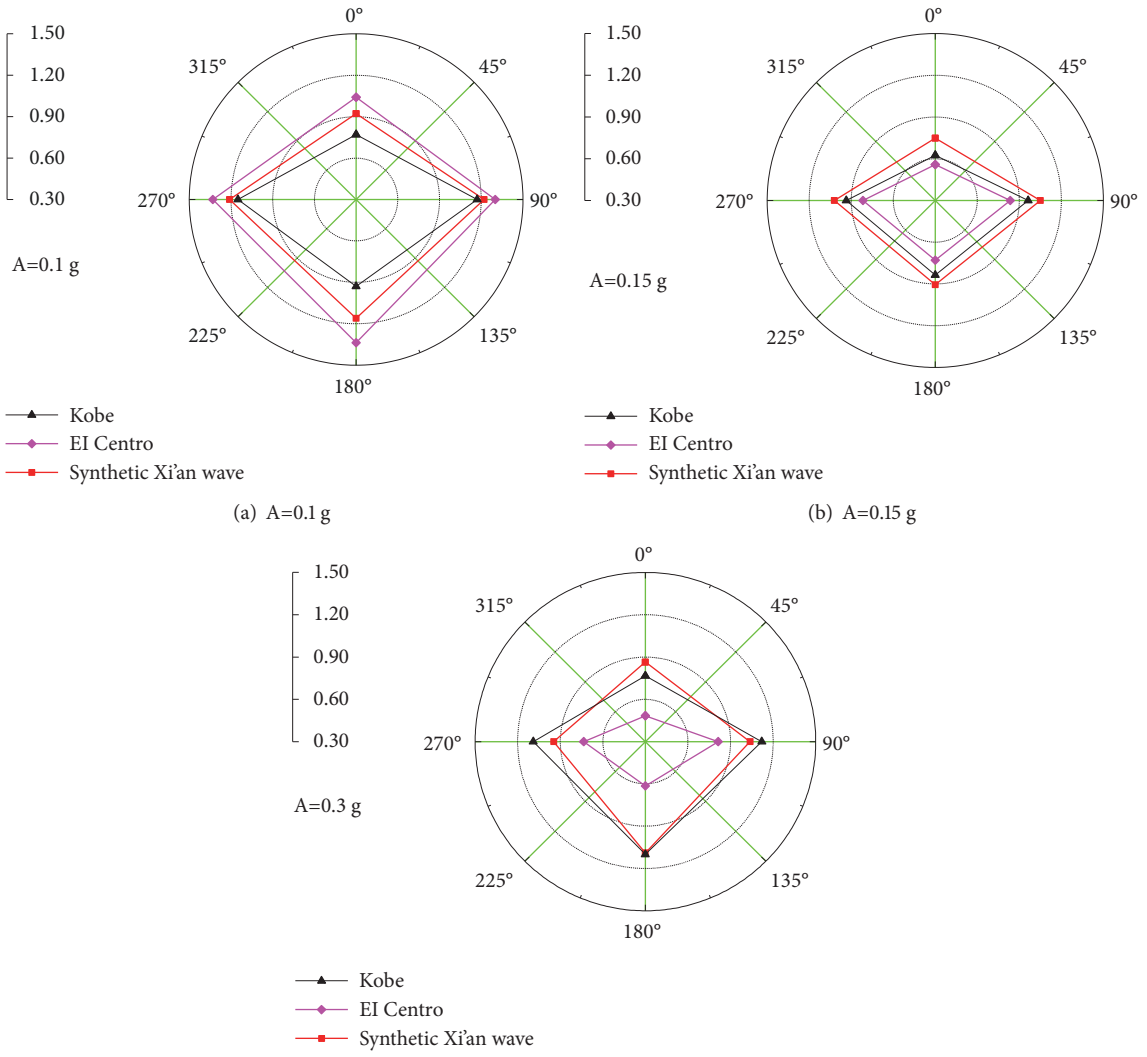

Figure 8: Acceleration amplifying coefficient of tunnel.

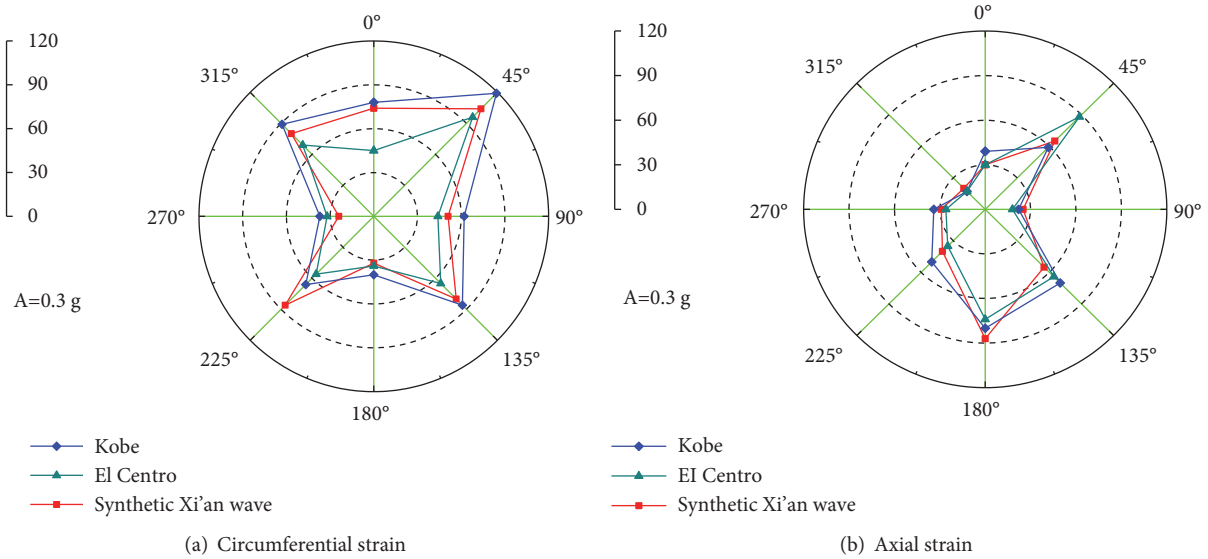

Figure 9: Radar map of dynamic strain.

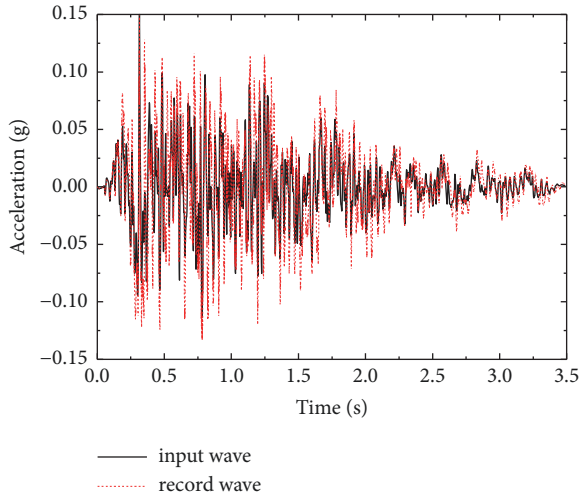

Figure 10: Acceleration time history waves.

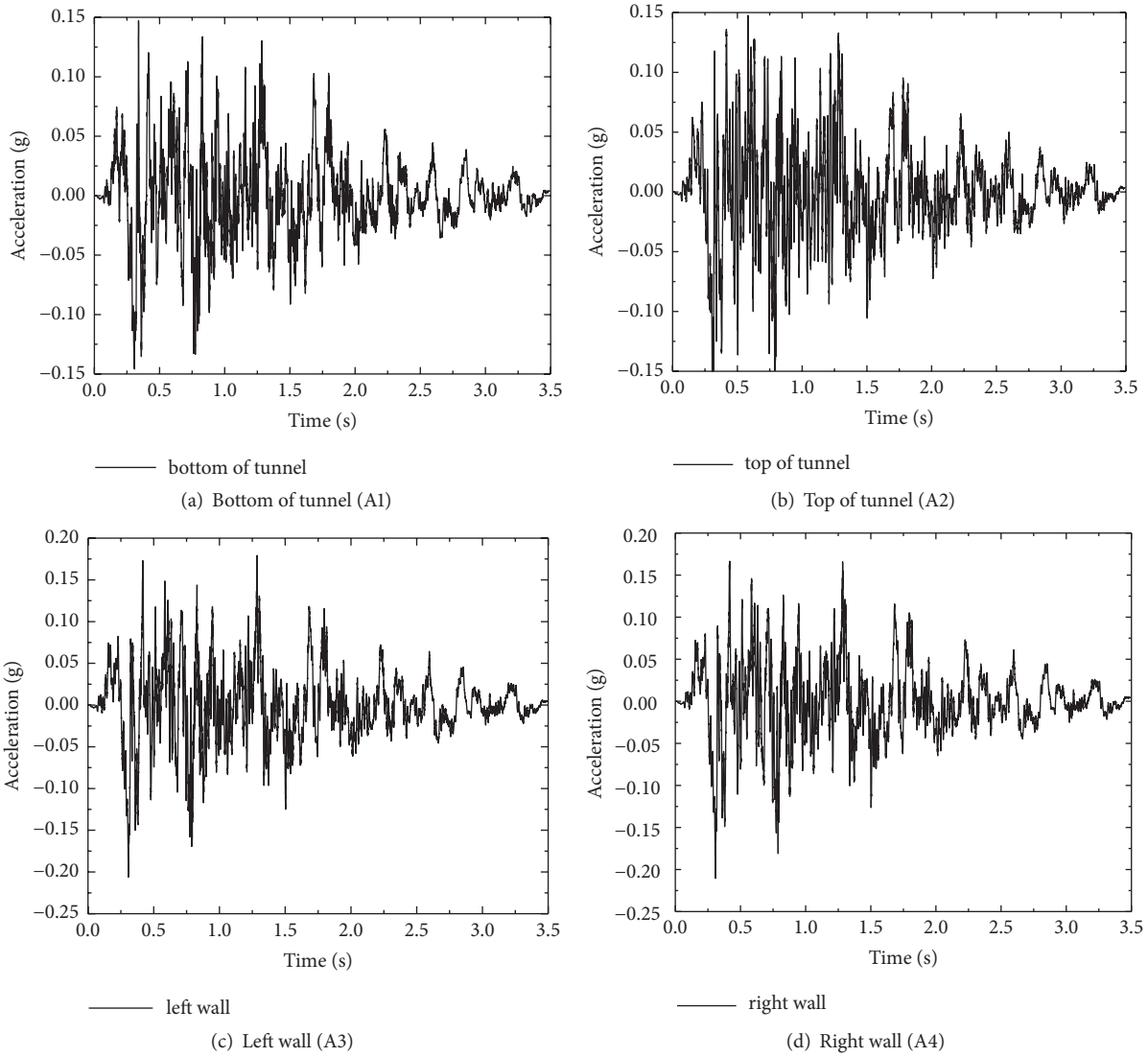

(a) Bottom of tunnel (A1)

(b) Top of tunnel (A2)

(c) Left wall (A3)

(d) Right wall (A4)

Figure 11: Acceleration time history curve of tunnel.

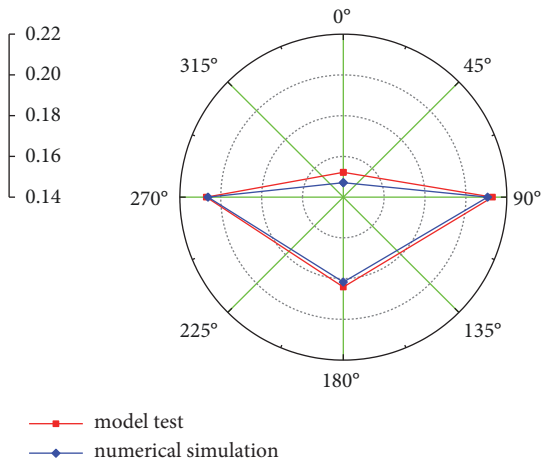

Figure 12: Radar map of peak acceleration.

wall, while the left part was a little faraway form the fissure. The peak acceleration at the top of the tunnel was the least one. The tunnel had scattering and emission effect with the transport of the earthquake wave from bottom to top tunnel. So the top of the tunnel had less peak acceleration than other parts. The influence of the fissure strengthens the dynamic effect of earthquake.

4. Conclusion

(1) The acceleration amplifying coefficient was bigger in the right wall than that in the symmetrically left wall. Average incremental percentage of acceleration amplifying coefficient was 8.33% from right wall to left wall. The right wall of tunnel was close to the fissure, but the left one was a little far away. The acceleration amplifying coefficient is determined by the distance to the fissure. The more close to the fissure, the greater the acceleration amplifying coefficient.

(2) The circumferential dynamic strain in the tunnel is influenced by the distance to the fissure. The biggest circumferential dynamic strain was 108 on the right wall (90°), while the least one was 18 at the 315° points of the left wall. The part of the tunnel which was close to the fissure had serious circumferential dynamic strain than that far away from the fissure. The axial dynamic strains along the tunnel were near equal no matter close or far from the fissure. The distance to fissure influenced the axial dynamic strain less.

(3) The numerical analysis results had a good correspondence with those of the shaking table model test. The waves had more scattering and emission effect at the top of tunnel. And the waves superposed at the top of the tunnel too. The superposition effect changes the shape of the wave at the top of the tunnel. The peak acceleration at the right wall was the biggest. The fissure increased the earthquake effect on tunnel.

Data Availability

The data in the article is obtained directly from the tests and the software. So the data in the article is direct data and is reliable.

Conflicts of Interest

The authors declare that they have no conflicts of interest.

Acknowledgments

This research is supported by the National Natural Science Foundation of China (41502277, 41630634, 41877250, 41772274), the Fund of Key Laboratory of Mine Geological Hazards Mechanism and Control (2017KF06), the Special Fund for Basic Scientific Research of Central Colleges, Chang'an University (300102269503, 300102269504), Natural Science Innovation Foundation of Department of Education of Guangdong Province (2016KTSCX001), the National Basic Research Program of China (973 Program: 2014CB744700), and the Fund of China Geological Survey (DD20160264). All supports are gratefully acknowledged.

References

[1] N. Liu, Q.-B. Huang, Y.-J. Ma, R. Bulut, and W. Fan, "Experimentalstudy of a segmental metro tunnel in a ground fissure area," *Soil Dynamics and Earthquake Engineering*, vol. 100, pp. 410–416, 2017.

[2] J. Peng, Q. Huang, Z. Hu et al., "A proposed solution to the ground fissure encountered in urban metro construction in Xi'an, China," *Tunnelling and Underground Space Technology*, vol. 61, pp. 12–25, 2017.

[3] N. Liu, Q.-B. Huang, W. Fan, Y.-J. Ma, and J.-B. Peng, "Seismic responses of a metro tunnel in a ground fissure site," *Geomechanics and Engineering*, vol. 15, no. 2, pp. 775–781, 2018.

[4] N. Liu, Q. Huang, L. Wang, W. Fan, Z. Jiang, and J. Peng, "Dynamic characteristics research of a ground fissure site at Xi'an, China," *Tunnelling and Underground Space Technology*, vol. 82, pp. 182–190, 2018.

[5] N. Liu, X. Feng, Q. Huang et al., "Dynamic characteristics of a ground fissure site," *Engineering Geology*, vol. 248, pp. 220–229, 2019.

[6] K. Kongai, H. Kamiya, and S. Nishiyama, "Deformation buildup in soil during the Kobe earthquake of 1995," *Seism. Fault-Introduced Failures*, vol. 1, pp. 81–90, 2001.

[7] W. C. Cheng, Z. P. Song, W. Tian, and Z. F. Wang, "Shield tunnel uplift and deformation characterisation: a case study from Zhengzhou metro," *Tunnelling and Underground Space Technology*, vol. 79, pp. 83–95, 2018.

[8] T. Sun, Z. Yue, B. Gao, Q. Li, and Y. Zhang, "Model test study on the dynamic response of the portal section of two parallel tunnels in a seismically active area," *Tunnelling and Underground Space Technology*, vol. 26, no. 2, pp. 391–397, 2011.

[9] K. Cui, J. Feng, and C. Zhu, "A study on the mechanisms of interaction between deep foundation pits and the pile foundations of adjacent skewed arches as well as methods for deformation control," *Complexity*, vol. 2018, Article ID 6535123, 19 pages, 2018.

[10] J. Zhang, J. Cao, L. Mu, L. Wang, and J. Li, "Buoyancy force acting on underground structures considering seepage of confined water," *Complexity*, vol. 2019, Article ID 7672930, 10 pages, 2019.

[11] Y. Cai, B. Tu, J. Yu, Y. Zhu, and J. Zhou, "Numerical simulation study on lateral displacement of pile foundation and construction process under stacking loads," *Complexity*, vol. 2018, Article ID 2128383, 17 pages, 2018.

[12] M. Jesmani, M. Kamalzare, and B. B. Sarbandi, "Seismic response of geosynthetic reinforced retaining walls," *Geomechanics and Engineering*, vol. 10, no. 5, pp. 635–655, 2016.

[13] Z. Angin, "Geotechnical field investigation on giresun hazelnut licenced warehause and spot exchange," *Geomechanics and Engineering*, vol. 10, no. 4, pp. 547–563, 2016.

[14] C.-H. Chen, T.-T. Wang, F.-S. Jeng, and T.-H. Huang, "Mechanisms causing seismic damage of tunnels at different depths," *Tunnelling and Underground Space Technology*, vol. 28, no. 1, pp. 31–40, 2012.

[15] W. Cheng, J. C. Ni, and S. Shen, "Experimental and analytical modeling of shield segment under cyclic loading," *International Journal of Geomechanics*, vol. 17, no. 6, Article ID 04016146, 2017.

[16] W. Yang, L. Li, Y. Shang et al., "An experimental study of the dynamic response of shield tunnels under long-term train loads," *Tunnelling and Underground Space Technology*, vol. 79, pp. 67–75, 2018.

[17] W. Yang, M. Hussein, and A. Marshall, "Centrifuge and numerical modeling of ground-borne vibration from an underground tunnel," *Soil Dynamics and Earthquake Engineering*, vol. 51, pp. 23–34, 2013.

[18] R. Y. S. Pak and B. B. Guzina, "Dynamic characterization of vertically loaded foundations on granular soils," *Journal of Geotechnical Engineering*, vol. 121, no. 3, pp. 274–286, 1995.

[19] G. Chen, Z. Wang, X. Zuo, X. Du, and H. Gao, "Shaking table test on the seismic failure characteristics of a subway station structure on liquefiable ground," *Earthquake Engineering & Structural Dynamics*, vol. 42, no. 10, pp. 1489–1507, 2013.

[20] F. Goktepe, E. Celebi, and A. J. Omid, "Numerical and experimental study on scaled soil-structure model for small shaking table tests," *Soil Dynamics and Earthquake Engineering*, vol. 119, pp. 308–319, 2019.

[21] W. Cheng, Z. Song, W. Tian, and Z. Wang, "Shield tunnel uplift and deformation characterisation: a case study from zhangzhou metro," *Tunnelling and Underground Space Technology*, vol. 79, pp. 83–95, 2018.